

The nature of the multi-wavelength emission of 3C 111

S. de Jong¹, V. Beckmann¹ and F. Mattana¹

François Arago Centre, APC, Université Paris Diderot, CNRS/IN2P3, CEA/Irfu, Observatoire de Paris, Sorbonne Paris Cité, 10 rue A. Domon et L. Duquet, 75205 Paris Cedex 13, France
e-mail: dejong@in2p3.fr

Accepted 13 July 2012

ABSTRACT

Aims. In order to determine the nature of the high energy emission of the radio galaxy 3C 111, we aim to disentangle the thermal and non-thermal processes.

Methods. We study the X-ray spectrum of 3C 111 between 0.4 and 200 keV, and its spectral energy distribution, using data from the Suzaku satellite combined with INTEGRAL, Swift/BAT data and Fermi/LAT data. Then, we model the overall spectral energy distribution including radio and infrared data.

Results. The combined Suzaku, Swift and INTEGRAL data are represented by an absorbed exponentially cut-off power law with reflection from neutral material with a photon index $\Gamma = 1.68 \pm 0.03$, a high-energy cut-off $E_{\text{cut}} = 227_{-67}^{+143}$ keV, a reflection component with $R = 0.7 \pm 0.3$ and a Gaussian component to account for the iron emission line at 6.4 keV with an equivalent width of $EW = 85 \pm 11$ eV. The X-ray spectrum appears dominated by thermal, Seyfert-like processes, but there are also indications for non-thermal processes. The radio to γ -ray spectral energy distribution can be fit with a single-zone synchrotron-self Compton model, with no need for an additional thermal component.

Conclusions. We suggest a hybrid scenario to explain the broad-band emission, including a thermal component (iron line, reflection) which dominates in the X-ray regime and non-thermal one to explain the spectral energy distribution.

Key words. galaxies: active – galaxies: individual: 3C 111 – X-rays: galaxies – gamma rays: galaxies

1. Introduction

Radio galaxies are a subclass of Active Galactic Nuclei (AGN) and in the unification model of AGN radio galaxies are the radio-loud counter parts of Seyfert galaxies (Antonucci 1993; Urry & Padovani 1995). For both of these classes it is thought that the inclination is large, such that the observer views the core, which is dominated by thermal processes through absorbing material. This is different for blazars, where the inclination angle is very small. The observed emission originates in the relativistic jet, which is dominated by non-thermal processes. Due to the Doppler boosting of the emission in the jet, the energy of the observed emission from blazars can reach the γ -ray regime, even up to TeV energies. Recently it has been discovered that several non-blazar AGN also emit significantly in the γ -ray regime (Hartman et al. 2008; Abdo et al. 2010c; Ackermann et al. 2011). Although there have been several theories (i.e. misaligned jet, shocks in the radio lobes) about the origin of this high-energy radiation, conclusive evidence for any of these theories is yet to be found.

3C 111 is a nearby ($z=0.049$, Sargent 1977) flat-spectrum FR-II radio galaxy (Fanaroff & Riley 1974; Linfield & Perley 1984). The source shows strong broad emission lines in the optical (Sargent 1977) and an iron emission line in the X-ray regime (Lewis et al. 2005), similar to Seyfert galaxies. In the radio regime the emission is dominated by the relativistic jet, which has an angle of 18° to our line of sight (Jorstad et al. 2005). The projected size of the jet is 78 kpc (Bridle & Perley 1984). There is no visible counter jet, but there is a bright lobe detectable in the opposite direction of the observed jet which is likely fed by the undetected counter jet (Linfield & Perley 1984).

Earlier studies of 3C 111 in the X-ray band have shown a high

energy cut-off of the spectrum. Dadina (2007) found a lower limit of $E_{\text{cut}} \geq 82$ keV using *BeppoSAX* data and Ballo et al. (2011) derived a similar lower limit on the cut-off of $E_{\text{cut}} \geq 75$ keV using data from *XMM-Newton* and *Suzaku/XIS* and PIN. Molina et al. (2009), using *XMM-Newton*, *Swift* and *INTEGRAL* data, constrained the cut-off energy at $E_{\text{cut}} = 126_{-50}^{+193}$ keV. It is uncertain if a reflection component is present in the X-ray spectrum. An upper limit of $R \leq 2.25$ was found by Dadina (2007) using *BeppoSAX* and constraints of $R = 0.9 \pm 0.6$ have been derived by Molina et al. (2009) and $R = 0.35 \pm 0.06$ by Ballo et al. (2011) using *Suzaku/XIS* and PIN. Ballo et al. (2011) also used *XMM-Newton* data to find the reflection between 0.4–10 keV to be $R = 0.19_{-0.04}^{+0.05}$. Rivers et al. (2011) did not detect a reflection component, using *RXTE* data between 3 and $\gtrsim 100$ keV. The equivalent width of the iron line at 6.1 keV has been measured several times and is likely variable. Ballo et al. (2011) and Tombesi et al. (2010) found similar values, $EW = 75 \pm 13$ eV (*Suzaku/XIS* and PIN) and $EW = 86 \pm 16$ eV (*Suzaku/XIS*), respectively. Using *Suzaku/XIS* data of three different observations taken two years later Tombesi et al. (2011) found a lower value for the EW , between $EW > 33$ eV and $EW > 40$ eV. Similarly, Ballo et al. (2011) also used *XMM-Newton* to fit the 0.4–10 keV spectrum and found an $EW = 38_{-9}^{+11}$ eV.

3C 111 has been detected in γ -rays by *CGRO/EGRET* (Hartman et al. 1999; Sguera et al. 2005; Hartman et al. 2008). It was included in the first *Fermi/LAT* catalogue (Abdo et al. 2010a). In the second *Fermi/LAT* catalogue the source was omitted since it was no longer significantly detected (Nolan et al. 2012). 3C 111 is likely variable in the γ -ray regime (Ackermann et al. 2011). Using 24 months of *Fermi/LAT* data Grandi et al. (2012) found 3C 111 to be detectable during a short

time period ($\Delta t \sim 30 - 60$ days), limiting the emission region to $R < 0.1$ pc (assuming a Doppler factor of $\delta = 3$) due to causality arguments. The detectability of the source in the GeV range coincided with an increase in the flux in the millimeter, optical and X-rays regime, indicating the emission is likely to emerge from the same region. Since the outburst in millimeter, optical and X-rays is associated with the ejection of a bright radio knot, this indicates that the GeV emission originates from the radio core within 0.3 pc from the central supermassive black hole.

To understand the physical processes which cause the emission in 3C 111, we first study the X-ray to γ -ray spectrum to find whether the emission is the product of thermal (Seyfert-like) or non-thermal processes (blazar-like) or a combination of both. Then, we model the Spectral Energy Distribution (SED) to understand the processes which dominate the broad-band radiation from radio to high energies of 3C 111.

2. Observations and data reduction

To cover a large energy band from X-rays to γ -rays to study the high-energy emission from 3C 111 we used data from several different instruments.

2.1. Suzaku-XIS/PIN

3C 111 was observed by Suzaku from 22 August 2008 to 25 August 2008 with a total elapsed time of 236.9 ks in HXD nominal pointing mode. We analysed data from the X-ray Imaging Spectrometer (XIS, Koyama et al. 2007) and Hard X-ray Detector (HXD, Takahashi et al. 2007). The XIS instrument consists of three separate CCD detectors and has an energy range from $\sim 0.2 - 12.0$ keV. The HXD is a collimated instrument, consisting of two independent detector systems; silicon PIN diodes which function between $\sim 10 - 60$ keV and GSO scintillation counters covering the energy range $\sim 30 - 600$ keV.

For the observations made with the XIS we used the clean events as provided by the instrument team where the standard event cuts have been applied.

The flux of 3C 111 is too low above 70 keV to extract a significant spectrum from the HXD/GSO detector, therefore we used only HXD/PIN data. The Suzaku team provides a response file for the PIN, which depends on the epoch in which the data were taken and on the pointing mode. Also a non X-ray background (NXB) per observation is available for the PIN analysis. After filtering the source and background files in time using the good time intervals we extracted the source and background spectra. The source spectrum needs to be corrected for dead time events, for this we use `HXDDECOR`. The NXB has been simulated with ten times more counts to suppress statistical errors. Therefore we needed to increase the exposure time of the background spectrum with a factor of ten. Using `XSPEC` we simulated the cosmic X-ray background (CXB) using the PIN response file for the flat emission distribution for the proper epoch and point mode. We combined the NXB and CXB files and used this as background in our analysis.

2.2. INTEGRAL IBIS/ISGRI

The INTEGRAL satellite is a gamma-ray observatory with several instruments on board. We used the INTEGRAL Soft Gamma-Ray Imager (ISGRI), a part of the Imager on Board INTEGRAL Spacecraft (IBIS), a coded-mask detector. ISGRI is sensitive between 15 keV to 1 MeV (Lebrun et al. 2003).

We have used all data collected by INTEGRAL since the launch of the satellite up to August 2009, with a total exposure time of 508 ks. We first created individual spectra for all science windows (a science window is all data produced during one pointing) using the `IBIS_SCIENCE_ANALYSIS` routine. Then we summed all the individual spectra to achieve a better signal to noise ratio.

2.3. Swift-BAT

The Burst Alert Telescope (BAT) aboard the Swift satellite is a coded-aperture camera with an energy range between 14–195 keV for imaging (Barthelmy et al. 2005). Since the BAT telescope is monitoring the sky continuously and has a large field of view (1.4 sr, partially coded), it has observed 3C 111 regularly. We used data from the 58-month hard X-ray survey, from 2004 December to the end of 2009 May (see Tueller et al. 2010; Baumgartner et al. 2010). The detected flux for 3C 111 in this survey is 1.2×10^{-10} erg cm $^{-2}$ s $^{-1}$ between 14 and 195 keV.

2.4. Fermi-LAT

The Large Area Telescope (LAT) aboard the Fermi satellite operates in an energy range between 20 MeV and 300 GeV (Atwood et al. 2009). The LAT is a pair-conversion telescope with a very wide field of view which scans the sky continuously. During the nominal all-sky survey observing mode of *Fermi*/LAT a total effective exposure time of 83.7 Ms was accumulated in the direction of 3C 111 between 4 August 2008 and 20 April 2011.

We selected the diffuse event class photons (P6_V3 instrument response functions) between 100 MeV and 200 GeV in a circular region of interest of 15° around the source. Events with a zenith angle of more than 105° are excluded (Abdo et al. 2009). We used the standard cuts as proposed by the Fermi team on the data quality of the events and instrument configuration.

The maximum likelihood analysis tool `GTLIKE` models all the emission in a given region which can contain several sources. The goodness of fit is expressed in the log-likelihood value; the probability of obtaining the data given an input model. After creating a model including all detectable sources in the field we used `GTLIKE` to fit the model until the log likelihood value was maximised. We found the test statistic value of 3C 111 to be $TS = 12.8$, which corresponds to a significance of $\sim 3\sigma$. The data provided only two significant points so it is not possible to fit the spectrum in e.g. `XSPEC`. However, when creating the spectrum, `GTLIKE` gives a spectral slope of $\Gamma_\gamma = 2.41 \pm 0.17$ between 0.1–200 GeV and a flux of $f = 1.2 \times 10^{-8}$ ph cm $^{-2}$ s $^{-1}$.

3. Results

3.1. X-ray spectrum

We simultaneously fitted the X-ray spectra, between 0.4 and 200 keV, in `XSPEC` (Arnaud 1996). We started our analysis by fitting the spectrum with an absorbed power law and a Gaussian component at 6.1 keV to account for the redshifted iron emission line. The fit resulted in a reduced chi-squared of $\chi_\nu^2 = 1.14$ (1678 d.o.f.). We tried to improve our fit by using a cut-off power law, which yielded a better fit with $\chi_\nu^2 = 1.12$ (1677 d.o.f.). We explored the possibility of a broken power law, but with a $\chi_\nu^2 = 1.14$ (1676 d.o.f.) this gave no improvement of the fit. Adding a reflection component did further improve the fit, $\chi_\nu^2 = 1.10$ (1676 d.o.f., F-test probability 4×10^{-8}). The resulting fit and the residuals are shown in Figure 1. We derived the following best-fit pa-

rameters and 90% errors: the value for the equivalent hydrogen column density $N_{\text{H}} = (9.0 \pm 0.2) \times 10^{21} \text{ cm}^{-2}$, a power law index of $\Gamma = 1.68 \pm 0.03$, a high-energy cut-off $E_{\text{cut}} = 227^{+143}_{-67} \text{ keV}$ and a reflection scaling factor $R = 0.7 \pm 0.3$. Figure 2 shows the confidence contours of the reflection component versus the cut-off energy with $\Delta\chi^2$ of 68%, 90% and 99.7%. We can exclude a cut-off below 130 keV at the 99.7% confidence level.

We have fit the data with a more physical model, compPS (Poutanen & Svensson 1996), which describes the process of thermal Comptonization. In this model seed photons from the cool thick accretion disc are injected in the electron plasma. The electron cloud can have several geometries, we chose a plane-parallel slab (we have applied other geometries as well but they did not influence the parameter values nor improve the fit). The electrons in the cloud have a Maxwellian distribution with an electron temperature T_e and an optical depth τ related to the Compton parameter $y = 4\tau kT_e / (m_e c^2)$. The seed photons will be up-scattered from their initial energy E_i to $E_f = e^y E_i$. The Compton scattering of the seed photons with the electrons in the plasma results in a spectrum which is afterwards reflected from a cool medium and then smeared out by the rotation of the disc. The best-fit model gave a $\chi^2_{\nu} = 1.10$ (1676 d.o.f.). The values we found for this model are: an equivalent hydrogen column density $N_{\text{H}} = (9.0 \pm 0.2) \times 10^{21} \text{ cm}^{-2}$, a temperature of the electrons $kT_e = 91^{+22}_{-48} \text{ keV}$, a reflection component $R = 1.8^{+0.5}_{-0.7}$ and a Compton parameter of $y = 0.6 \pm 0.1$ (which corresponds to an optical depth $\tau = 0.8$).

We also fitted all data sets individually with an absorbed power law and Gaussian component. The values of the flux levels and power law indices for these individual best fits for the data can be found in Table 1.

The measurements of the iron line at 6.4 keV are consistent in all three *Suzaku*/XIS spectra. After adding the three spectra together we derived a line energy $E_{\text{line}} = 6.11 \pm 0.02 \text{ keV}$ and an equivalent width of $EW = 85 \pm 11 \text{ eV}$.

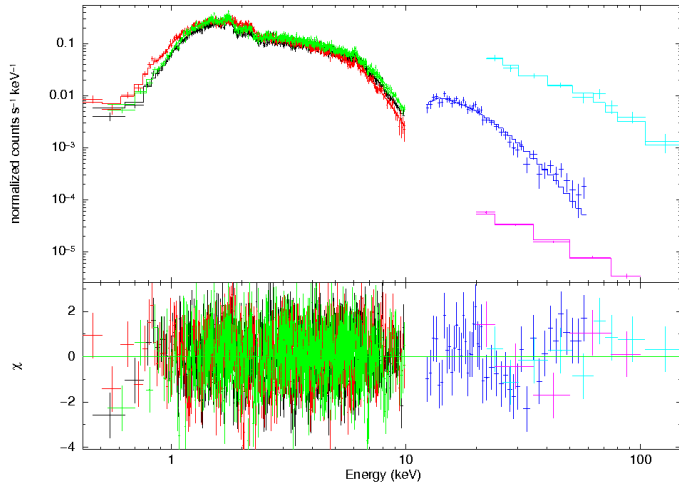


Fig. 1. The count spectrum of the combined *Suzaku*/XIS (0.4-10 keV), *Suzaku*/PIN (12-60 keV), INTEGRAL ISGRI (20-200 keV) and *Swift*/BAT (15-150 keV) data with the fitted model: an absorbed cut-off power law with reflection from neutral material and a Gaussian component to account for the iron line at 6.4 keV. The bottom panel shows the residuals in terms of sigma with error bars of size one.

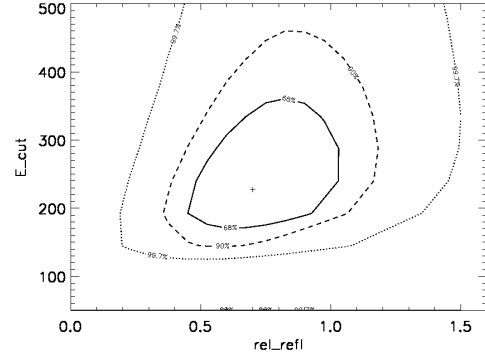


Fig. 2. Error contours for the best-fit pexrav model, reflection component R vs the high-energy cut-off E_{cut} . The contour levels correspond to $\Delta\chi^2$ of 68%, 90% and 99.7% statistical confidence regions. A cut-off below 130 keV is excluded on a 99.7% level.

3.2. Fitting of the time-averaged SED

After we created a spectral energy distribution (SED) based on our data, we modelled it with a public synchrotron self-Compton (SSC) code made by Krawczynski et al. (2004)¹. The SSC mechanism assumes an isotropic population of high-energy electrons that emit synchrotron radiation followed by inverse Compton scattering of the synchrotron photons to higher energies (Maraschi et al. 1992). The inverse Compton component may also include a thermal component of external seed photons (e.g. from the broad-line region or accretion disc) that are also Compton up scattered to high energies (external Compton component, Dermer & Schlickeiser 1993). The electron population is located in a spherical volume with radius R_s with a randomly oriented magnetic field B that moves relativistically towards the observer with a bulk Lorentz factor Γ and an angle between the jet and the line of sight θ . Thus the radiation is Doppler-shifted with a Doppler factor $\delta = [\Gamma(1 - \beta \cos \theta)]^{-1}$. The electron energy spectrum in the jet-frame follows a broken power law, with indices p_1 and p_2 , and is characterised by a minimum and maximum energy ($E_{\text{min}}, E_{\text{max}}$) and a break energy (E_{br}). The power in the SED is mostly influenced by the Doppler factor and the radius and magnetic field of the emitting region. The shape of the synchrotron and inverse Compton peaks and the peak frequencies depend strongly on the energies which define the electron population.

Since we only have data in the X-ray and γ -ray regime it is not possible to model the entire SED. Therefore we have added archival radio data (where we neglected the observations that only included the core) and infrared data from the NED archive². Assuming that the infrared emission is produced in the same region as the X-rays (the accretion disc or inner jet), we can use the column density found in the X-ray spectra, $N_{\text{H}} = 9.0 \times 10^{21} \text{ cm}^{-2}$ to calculate the extinction in the V-band $A_{\text{V}} = N_{\text{H}} / (1.79 \times 10^{21} \text{ cm}^{-2})$ (Predehl & Schmitt 1995). From the extinction in the V-band we can calculate the extinction in the near-infrared bands J, H and K using the correction factors from Schlegel et al. (1998). We removed the *Suzaku*/XIS data below 1 keV to avoid possible contamination by star burst emission.

Using our best fit of the X-ray spectrum we can constrain some of the parameters. The indices of the power law are tied to the

¹ <http://jelly.wustl.edu/multiwave/spectrum/?code>

² <http://ned.ipac.caltech.edu/>

Table 1. The parameters for the individual power law fits of the data, and their 90% confidence level.

Instrument	Epoch	Exposure time	PL index	f [erg cm ⁻² s ⁻¹]	Energy range
XIS0	22-25 August 2008	95.4 ks	1.60 ± 0.02	$(2.20 \pm 0.02) \times 10^{-11}$	0.4–10 keV
XIS1	22-25 August 2008	95.4 ks	1.59 ± 0.02	$(2.24^{+0.03}_{-0.02}) \times 10^{-11}$	0.4–10 keV
XIS3	22-25 August 2008	95.4 ks	1.63 ± 0.02	$(2.2 \pm 0.02) \times 10^{-11}$	0.4–10 keV
PIN	22-25 August 2008	101.9 ks	1.52 ± 0.14	$(4.8 \pm 0.4) \times 10^{-11}$	12–60 keV
ISGRI	24 March 2003-19 August 2009	508 ks	1.90 ± 0.20	$(1.2 \pm 0.2) \times 10^{-10}$	20–200 keV
BAT	December 2004-May 2009	54 months ^a	1.99 ± 0.09	$(1.05 \pm 0.05) \times 10^{-10}$	15–150 keV
LAT	4 August 2008-20 April 2011	83.7 Ms	2.4 ± 0.2	$(6 \pm 2) \times 10^{-12}$	> 100 MeV

Notes. ^(a) Elapsed time

power law index of the X-ray spectrum: the first power law index is $p_1 = 2$ (below E_{br}). Starting with this parameter and the initial parameters of the code, we optimised the model. We focused on the energies that characterise the electron population to shape the peaks, and to change the overall energy output in the SED we adjusted the radius of the emitting region, its magnetic field and Doppler factor.

We found that the break in the electron power law is not significant and therefore we use a single power law with index $p_1 = p_2$. Furthermore we found the minimum energy of the electron distribution to be $E_{min} = 5.6 \times 10^6$ eV and the maximum energy $E_{max} = 6.8 \times 10^9$ eV. The Doppler factor is $\delta = 14$, the radius of the spherical emission volume is $R_s = 2 \times 10^{16}$ cm and a magnetic field of $B = 4 \times 10^{-2}$ G. The parameters we used to fit the data can be found in Table 2, and the resulting plot in Figure 3. The addition of an external Compton component does not improve the model.

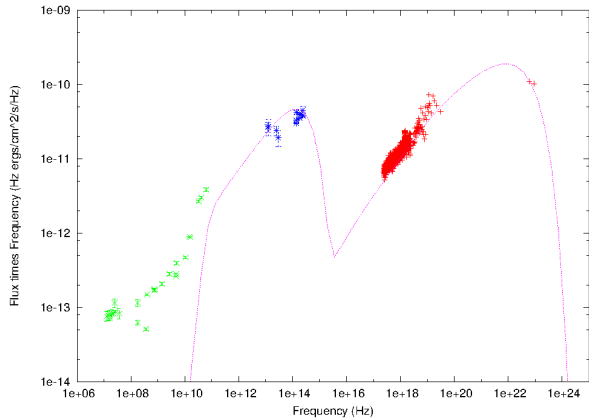


Fig. 3. SED showing 3C 111 unabsorbed fluxes and the SSC one-zone model. Crosses indicate data extracted and analysed in this work. We have added archival, deabsorbed IR and radio points from NED. The line shows the SSC model. See Table 2 for the values used.

4. Discussion

In order to evaluate the physical processes that dominate the high-energy emission from X-ray to γ -rays in 3C 111 we have studied the X-rays spectrum and the broad-band spectral energy distribution.

4.1. X-ray spectrum

We have constrained the high-energy cut-off of 3C 111 by applying the `pexrav` model, which describes an exponentially cut-off power law spectrum reflected from neutral material (Magdziarz & Zdziarski 1995) in `xSPEC`. We found a cut-off $E_{cut} = 227^{+143}_{-67}$ keV using data from *INTEGRAL*/ISGRI, *Suzaku*/XIS and PIN and *Swift*/BAT. The indication of the cut-off can already be seen in the power law indices of the individual fits, which go from $\Gamma \sim 1.6$ in the soft X-rays to ~ 1.9 in the hard band (Table 1). We have also applied the physical `compPS` model to the same data, which yielded an electron temperature $kT_e = 91^{+22}_{-48}$ keV, which relates to the cut-off energy via $E_{cut} \approx 3kT_e$. The electron temperature we found using the `compPS` model is consistent with the cut-off energy we derived using the `pexrav` model.

The value we found for the high-energy cut-off is consistent with upper limits reported by Dadina (2007) and Ballo et al. (2011) and the measurement by Molina et al. (2009). Rivers et al. (2011) found, using data from *RXTE* from 3 to $\gtrsim 100$ keV, that the addition of a cut-off does not improve their fit of 3C 111. This might be due to the fact we used a combination of different instruments and a larger energy range for the spectrum presented here.

A high-energy cut-off is a property of the high-energy spectrum of Seyfert galaxies and the value we have derived for 3C 111 is in the expected range for cut-off energies observed in Seyferts (Beckmann et al. 2009; Dadina 2008).

We have measured reflection in 3C 111 by using both the `compPS` and the `pexrav` model, $R = 1.8^{+0.5}_{-0.7}$ and $R = 0.7 \pm 0.3$ respectively. Since these models are very different (`pexrav` is a descriptive model and `compPS` is a physical model) it is not unexpected to find different measures of the reflection. Beckmann et al. (2011) have applied both models to the hard X-ray spectrum of the radio galaxy Cen A and found the reflection in the case of `compPS` also to be slightly higher though consistent with reflection found using the `pexrav` model.

The reflection scaling factor we got, $R = 0.7 \pm 0.3$ using the `pexrav` model can be compared to earlier work using the same model. Our results are consistent with an upper limit reported by Dadina (2007), as well as with constraints by Molina et al. (2009) and Ballo et al. (2011). The latter also reported a significantly lower result, $R = 0.19^{+0.05}_{-0.04}$, when using only soft X-ray data between 0.4 and 10 keV. This is to be expected since the reflection component is dependent on the energy band used to observe it. Also Rivers et al. (2011) did not detect a reflection component when applying the `pexrav` model between 3 and $\gtrsim 100$ keV. They forced the model to avoid a high-energy cut-off which

Table 2. Parameters used to model the SED of 3C 111 using the code by Krawczynski et al. (2004). For comparison we include the fit parameters for the core of Centaurus A (Abdo et al. 2010b) and Markarian 421 (low flux state, Błażejowski et al. 2005).

Symbol	Description	3C 111	Cen A	Mrk 421
δ	Doppler factor	14	1.0	10.0
R_s	Radius of the emission volume [cm]	2×10^{16}	3.0×10^{15}	7.0×10^{15}
B	Magnetic field of emission volume [G]	4×10^{-2}	6.2	0.405
E_{\min}	Minimum energy of the electron distribution [eV]	5.6×10^6	1.5×10^8	3.2×10^6
E_{\max}	Maximum energy of the electron distribution [eV]	6.8×10^9	5.0×10^{13}	1.7×10^{11}
E_{br}	Break energy of the electron distribution [eV]	-	4.0×10^8	2.2×10^{10}
p_1	Spectral index of electron spectrum (E_{\min} to E_{br})	2	1.8	2.05
p_2	Spectral index of electron spectrum (E_{br} to E_{\max})	-	4.3	3.6
$\log L$	Bolometric Luminosity (3-200 keV) [erg s $^{-1}$]	44.7	42.5 ^a	45.5 ^b

Notes. ^(a) Beckmann et al. (2011); ^(b) Lichti et al. (2008)

might explain the difference compared to our result.

The value we measured is also consistent with average Seyfert properties; $R = 1.2^{+0.6}_{-0.3}$ for Seyfert 1 and $R = 1.1^{+0.7}_{-0.4}$ for Seyfert 2 galaxies (Beckmann et al. 2009).

The equivalent width of the iron line at 6.11 keV we found to be $EW = 85 \pm 11$ eV, similar to the results of Ballo et al. (2011) and Tombesi et al. (2010). Lower values between $EW > 33$ eV and $EW > 40$ eV have been reported by Tombesi et al. (2011). Since the source is variable it is likely for the iron line EW to vary depending on the continuum. Figure 4 shows the correlation between the flux between 4 and 10 keV and the EW of the iron line for several observations. The correlation between the flux and the EW has a significance of $> 95\%$, Pearson's test coefficient is $r = -0.3$ and Spearman's rank correlation coefficient $r_s = -0.7$, showing a believable correlation between the flux level and the EW. If we do not consider the high equivalent width measurement based on *RXTE* data presented by Rivers et al. (2011) we get a highly significant correlation with a probability of $> 99\%$. Tombesi et al. (2010, 2011) also report the power law indices changing for the different data sets. Similarly, using a different data set, Ballo et al. (2011) derived an $EW = 38^{+11}_{-9}$ eV. Again, since there is a difference of several months between both data sets this value can be explained by the source variability. The value we found for the equivalent width is lower than the average value for Seyfert galaxies Dadina (2008): $EW = 448 \pm 67$ eV, the average for Seyfert 1 being $EW = 222 \pm 33$ eV and for Seyfert 2 $EW = 693 \pm 195$ eV. The correlation between equivalent width of the iron line and the underlying power law flux indicates that the line flux does not vary significantly whereas the continuum varies by a factor of 5. This can be naturally explained if the majority of the continuum flux is produced in a non-thermal and variable process. The low value of the EW of the iron line might indicate that the X-ray spectrum of 3C 111 does not only show a thermal, but also a non-thermal contribution.

We have also fitted the spectrum with the physical compPS model, deriving a temperature for the electron cloud $kT_e = 91^{+22}_{-48}$ keV, a Compton parameter $y = 0.6 \pm 0.1$ (which corresponds to an optical depth of $\tau = 0.8$) and a reflection component $R = 1.8^{+0.5}_{-0.7}$.

NGC 4151 is a well-studied case of a Seyfert core at hard X-rays. Beckmann et al. (2005) have used the compPS model on the spectrum of the Seyfert galaxy NGC 4151 between 2-300 keV. They found for the electron plasma temperature $kT_e = 94^{+4}_{-10}$ keV, a reflection component $R = 0.72 \pm 0.14$ and an optical

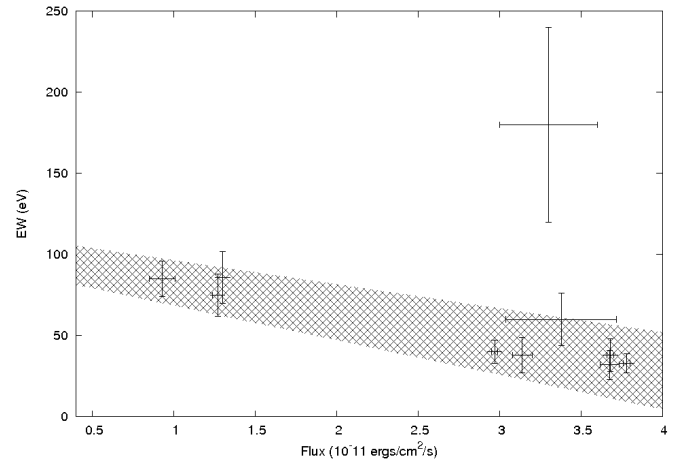


Fig. 4. Flux of the source versus the equivalent width of the iron line. Data taken from Tombesi et al. (2010, 2011); Ballo et al. (2011); Lewis et al. (2005); Rivers et al. (2011); Eracleous et al. (2000) and this work are plotted in points with error bars. We used a linear regression fit to derive a correlation between the two parameters. The fit is plotted with grey dashed lines indicating the 1σ error region.

depth of $\tau = 1.3^{+0.13}_{-0.05}$. The hard X-ray spectrum (3–1000 keV) of Centaurus A, which is another nearby γ -ray detected radio galaxy, has also been modelled with compPS (Beckmann et al. 2011). This yielded an electron plasma temperature of $kT_e = 206 \pm 62$ keV, a Compton parameter $y = 0.42^{+0.09}_{-0.06}$ (which corresponds to an optical depth of $\tau = 0.26$) and a reflection component of $R = 0.12^{+0.09}_{-0.10}$. NGC 4151 is optically thick, whereas both Cen A and 3C 111 are not. The optical thickness of NGC 4151 is dependent on the flux state and can go down to $\tau \sim 0.3 - 0.6$ in the dim state (Lubiński et al. 2010). In this state the electron temperature can increase to $T_e \sim 180 - 230$ keV. The optical depth of 3C 111 is similar to the dim state of NGC 4151, but the electron temperature is closer to the electron temperature of the brighter state. The reflection measured in 3C 111 is higher than found in both NGC 4151 and Cen A.

Chatterjee et al. (2011) concluded that the X-ray spectrum of 3C 111 is of thermal inverse Compton origin, based on a correlation between the optical and X-ray flux, as well as a weak optical polarisation and a smaller variance of the optical com-

pared with X-ray flux at shorter time scales. They conclude that these findings are consistent with a reprocessing model where the X-rays are mostly produced by inverse Compton scattering of thermal optical/UV seed photons from the accretion disc. The cut-off we measure using the `pexrav` model can be either thermal or non-thermal. It can be interpreted as a high-energy cut-off measured in Seyfert galaxies. In the case of 3C 111 the cut-off value is also comparable to typical cut-offs found in Seyfert galaxies. The cut-off observed in the `pexrav` model can also be caused by non-thermal inverse Compton scattering processes. In this case, the smooth turn-over of the inverse Compton branch towards higher energies appears as a cut-off in the `pexrav` model. Whereas in the thermal inverse Compton case the cut-off is exponential, the non-thermal spectrum is curved in a way that gamma-ray and VHE emission are not excluded. To differentiate between an exponential and a simple cut-off in the hard X-rays is not possible based on the data at hand, thus both the non-thermal and the thermal interpretation of the curved X-ray spectrum are still valid. The reflection component is a property of Seyfert galaxies and a result of thermal processes. The reflection component we detect is in the typical range for reflection in Seyfert galaxies. The EW of the observed iron line is lower than expected from Seyfert galaxies. The EW is also variable, which suggests a variable continuum. Therefore we suggest that, while the thermal processes in the X-ray band in 3C 111 seem to dominate, we cannot exclude a non-thermal contribution.

4.2. γ -rays

3C 111 has been suggested as a counterpart for the γ -ray source 3EG J0416+3650 in the third *CGRO*/EGRET catalogue, however it fell outside of the 99% probability region (Hartman et al. 1999). A re-analysis of the data (Sguera et al. 2005) concluded that 3EG J0416+3650 is likely associated with 3C 111. Indeed, there are no other plausible counterparts in the EGRET error region, which is also larger than previously thought; the quoted errors were statistical only and did not take into account the larger systematic errors due to inaccuracies in the Galactic diffuse model. The EGRET data have been re-analysed (Hartman et al. 2008) and it has been found that 3EG J0416+3650 is likely to result from the blending of more than one source. One of these components (detected only above 1 GeV) can be associated with 3C 111. Furthermore 3C 111 was included in the first Fermi/LAT source catalogue (Abdo et al. 2010a) with a significance of 4.3σ . In the second Fermi/LAT source catalogue 3C 111 has been excluded because the source was no longer significantly detected (Nolan et al. 2012). However, 3C 111 is very likely to be variable (Ackermann et al. 2011) and therefore no longer detectable in the second year. This has also been confirmed by Kataoka et al. (2011), who find a significance $>5\sigma$ for 3C 111 using 24 months of Fermi/LAT data and by Grandi et al. (2012) who indeed find that the γ -ray emission is not persistent, but flaring and associated with the ejection of bright radio knots. Since 3C 111 has been detected by *CGRO*/EGRET and Fermi/LAT at different epochs we assume that the source is a variable γ -ray emitter. We included data from the first Fermi/LAT catalogue where the source has been detected significantly. Our analysis gives a power law index that is similar to that given in the first catalogue with a comparable flux level (Abdo et al. 2010a).

4.3. SED

To construct the SED of a variable source, simultaneous data are necessary in order to get an un-affected measurement. The data used in the SED of 3C 111 are not simultaneous, which can affect the results in the sense that the SED is composed out of measurements from different spectral states. This effect is more severe for very variable objects, whereas in most wavebands 3C 111 is moderately variable. See for example Beckmann et al. (2007) who found no significant variability in hard X-rays in a study of 9 months of *Swift*/BAT data. For the radio domain, Grossberger et al. (2012) present decade long light curves which show variations up to a factor of 2 which we can consider as nonsignificant variability in the context of the SED. Also for other radio galaxies it has been shown that the approach to use non-simultaneous data in order to construct the SED does not introduce a significant bias. For example, the radio galaxies NGC 1275 (Antón et al. 2004) and Pictor A (Brown & Adams 2012) have also been analysed similarly using time-averaged SEDs. The results on the physical parameters should thus not be significantly affected by the moderate variability of 3C 111. The archival radio data used to model the SED are not well-represented by our SSC model. For observatories that operate in different wavebands there is a large difference in the field of view and resolution. The resolution is dependent on the wavelength via $RL = \lambda/D$ with RL the resolution, λ the wavelength and D the dish diameter. Therefore it is possible that we probe different regimes in the broad-band SED, which the one-zone model does not account for.

In SSC models the relativistic electron energy distribution is often assumed to be a broken power law, with a break energy E_{br} , a power law index before the break $p_1 < 3$ and a power law index after the break $p_2 > 3$ (see for example Ghisellini et al. 1996; Tavecchio et al. 1998; Krawczynski et al. 2004). The electron population is confined in a region with a radius R_s and a magnetic field B that moves with a Doppler factor δ along the jet. The electrons emit synchrotron radiation and inverse Compton radiation using the synchrotron photons as seed photons. For electrons with energies below the break energy E_{br} , cooling of the electrons dominates and in the regime after the break escape of electrons from the source dominates. The peak synchrotron power is emitted by electrons at the break energy (Tavecchio et al. 1998). In the case of 3C 111 we found that using a broken power law gave a break energy of $E_{br} = 1.6$ GeV and power law indices $p_1 = 2$ and $p_2 = 2.2$. The break between the two power laws is not significant. Therefore we apply a single power law with an index $p = 2$, based on the power law index of the X-ray spectrum. In the case of a single power law the maximum synchrotron power is emitted near the maximum energy of $E_{max} \approx 7$ GeV.

The energies that define the electron distribution, E_{min} and E_{max} influence the shape of the synchrotron and inverse Compton peak and were chosen empirically. If the minimum energy, E_{min} , decreases the maximum of the peak occurs at lower frequency and the slopes are less steep. Increasing the E_{min} increases the depth between the synchrotron and inverse Compton peak and steepens the rise and fall of the peaks. The maximum energy, E_{max} , is tied to the peak frequencies of both the synchrotron and inverse Compton peak. Increasing the quantity would increase the peak frequencies.

Abdo et al. (2010b) have modelled the SED of the core of the radio galaxy Cen A, using simultaneous data from the radio up to the γ -ray regime, applying a single-zone SSC. Comparing the parameters for this model and our own (see Table 2) it is

clear that the models have significantly different parameter values. The magnetic field has a much higher value in the case of Cen A ($B = 6.2$ G), compared to the value we found for 3C 111 ($B = 0.04$ G). The higher magnetic field increases the resulting flux because the synchrotron power is dependent on the magnetic field. Contrarily, the Doppler factor used to model Cen A is low ($\delta = 1$) compared to the value we found for 3C 111, $\delta = 14$. A lower Doppler factor means that the emission is less boosted and therefore appears less energetic. There are also three orders of magnitude difference between the emission volumes, for Cen A $R_s = 3 \times 10^{15}$ cm was used whereas we assume $R_s = 2 \times 10^{16}$ cm for 3C 111. Since this defines the amount of particles this also causes the flux to be lower for Cen A than for 3C 111. The higher value used for the magnetic field is attenuated by the lower Doppler factor and radius for Cen A, which causes the overall output to be lower, as expected for the less luminous source.

Pictor A is another FR-II radio galaxy that has been detected by *Fermi*/LAT as reported by Brown & Adams (2012), who have modelled the SED of one of the hot-spots in the radio-lobe of Pic A with a one-zone SSC model using the same code we applied. They concluded that it is not possible to describe both the X-ray and γ -ray emission using the SSC model. Since the γ -ray emission is very variable it is likely to originate from the jet, whereas the X-rays originate from the hot-spot. This would indicate that more than one zone is needed to model the entire SED. Błażejowski et al. (2005) used also the Krawczynski code to model the high-energy peaked BL Lac object Mrk 421, assuming just an SSC component. The parameter values they derived are shown in Table 2. Both the Doppler factor ($\delta = 10$) and the emitting region radius ($R_s = 7 \times 10^{15}$ cm) chosen for Mrk 421 are smaller than those chosen for 3C 111, but are larger than those of Cen A. Similar to Cen A, the magnetic field value for Mrk 421, $B = 0.4$ G, is a factor of 10 larger than for 3C 111. The smaller radius and Doppler factor decrease the flux, but due to the strong magnetic field the flux in the SED for Mrk 421 is higher than the flux of 3C 111.

We conclude that the overall emission from 3C 111 can be modelled with a simple synchrotron self-Compton model, where no additional thermal Compton component is needed. Since the X-rays appear to be (mostly) from thermal origin the SED gives an upper limit on the non-thermal emission in the X-ray band. There might be a thermal component in the SED, but with the current data we are not able to disentangle the possible thermal component from the overall non-thermal emission.

5. Conclusion

The origin of the high-energy emission from non-blazar AGN is still a topic of discussion. Marscher et al. (2002) have suggested that with the acceleration of inner regions of the accretion disk a shock front will stream along the jet and the expulsion of a superluminal bright knot will follow. Grandi et al. (2012) show, using *Fermi*/LAT data, that the GeV emission of 3C 111 appears to originate from a compact knot confined within 0.1 pc. This knot is clearly separated from the core and is placed 0.3 pc from the central engine.

By analysing the X-ray spectrum and the broad-band spectral energy distribution we have studied the nature of the high-energy emission of the radio galaxy 3C 111. We have presented an X-ray spectrum of 3C 111 between 0.4 and 200 keV using several instruments and showed that the best fit model is an absorbed cut-off power law with a reflection component and a Gaussian component to account for the iron line at 6.4 keV. The values

we found for the reflection and high-energy cut-off are similar to those found in Seyfert galaxies, which would indicate a thermal core. The cut-off can also originate from non-thermal processes and the equivalent width of the iron line is variable and lower than expected from Seyfert galaxies. Therefore we conclude that the X-ray spectrum is mainly of thermal origin, but there might be a small non-thermal contribution.

Using the X-ray spectrum, together with γ -ray data from *Fermi*/LAT and archival deabsorbed radio and infrared data we modelled the broad-band spectral energy distribution of 3C 111 using a single-zone synchrotron self-Compton model. This model is non-thermal and we also did not need an additional thermal component to model the SED. Since the X-ray emission is likely to be of combined thermal and non-thermal origin the SSC model we used might overestimate the non-thermal contribution in the X-ray band and should therefore be considered an upper limit.

In conclusion it seems that the origin of the high-energy emission in 3C 111 consists of both a thermal and a non-thermal component. In the X-ray spectrum the thermal components manifest through the presence of an iron line and reflection. The non-thermal component is visible through the variability of EW of the iron line. The high-energy cut-off can be the result of either thermal or non-thermal inverse Compton scattering and the present spectrum does not allow to distinguish which process is occurring. The broadband SED can be modelled with a non-thermal model, but it is possible there is a thermal component which we are not able to discern with the current data set.

Acknowledgements. This research has made use of NASA's Astrophysics Data System Bibliographic Services. We acknowledge the use of public data from the Swift data archive. This research has made use of the NASA/IPAC Extragalactic Database (NED) which is operated by the Jet Propulsion Laboratory, California Institute of Technology, under contract with the National Aeronautics and Space Administration.

References

- Abdo, A. A., Ackermann, M., Ajello, M., et al. 2009, *ApJS*, 183, 46
- Abdo, A. A., Ackermann, M., Ajello, M., et al. 2010a, *ApJS*, 188, 405
- Abdo, A. A., Ackermann, M., Ajello, M., et al. 2010b, *ApJ*, 719, 1433
- Abdo, A. A., Ackermann, M., Ajello, M., et al. 2010c, *ApJ*, 720, 912
- Ackermann, M., Ajello, M., Allafort, A., et al. 2011, *ApJ*, 743, 171
- Antón, S., Browne, I. W. A., Marchã, M. J. M., Bondi, M., & Polatidis, A. 2004, *MNRAS*, 352, 673
- Antonucci, R. 1993, *ARA&A*, 31, 473
- Arnau, K. A. 1996, in *Astronomical Society of the Pacific Conference Series*, Vol. 101, *Astronomical Data Analysis Software and Systems V*, ed. G. H. Jacoby & J. Barnes, 17
- Atwood, W. B., Abdo, A. A., Ackermann, M., et al. 2009, *ApJ*, 697, 1071
- Ballo, L., Braitto, V., Reeves, J. N., Sambruna, R. M., & Tombesi, F. 2011, *MNRAS*, 418, 2367
- Barthelmy, S. D., Barbier, L. M., Cummings, J. R., et al. 2005, *Space Sci. Rev.*, 120, 143
- Baumgartner, W. H., Tueller, J., Markwardt, C., & Skinner, G. 2010, in *Bulletin of the American Astronomical Society*, Vol. 42, *AAS/High Energy Astrophysics Division #11*, 675
- Beckmann, V., Shrader, C. R., Gehrels, N., et al. 2005, *ApJ*, 634, 939
- Beckmann, V., Barthelmy, S. D., Courvoisier, T. J.-L., et al. 2007, *A&A*, 475, 827
- Beckmann, V., Soldi, S., Ricci, C., et al. 2009, *A&A*, 505, 417
- Beckmann, V., Jean, P., Lubiński, P., Soldi, S., & Terrier, R. 2011, *A&A*, 531, A70
- Błażejowski, M., Blaylock, G., Bond, I. H., et al. 2005, *ApJ*, 630, 130
- Bridle, A. H. & Perley, R. A. 1984, *ARA&A*, 22, 319
- Brown, A. M. & Adams, J. 2012, *MNRAS*, 2454
- Chatterjee, R., Marscher, A. P., Jorstad, S. G., et al. 2011, *ApJ*, 734, 43
- Dadina, M. 2007, *A&A*, 461, 1209
- Dadina, M. 2008, *A&A*, 485, 417
- Dermer, C. D. & Schlickeiser, R. 1993, *ApJ*, 416, 458
- Eracleous, M., Sambruna, R., & Mushotzky, R. F. 2000, *ApJ*, 537, 654

- Fanaroff, B. L. & Riley, J. M. 1974, MNRAS, 167, 31P
Ghisellini, G., Maraschi, L., & Dondi, L. 1996, A&AS, 120, C503
Grandi, P., Torresi, E., & Stanghellini, C. 2012, ApJ, 751, L3
Grossberger, C., Kadler, M., Wilms, J., et al. 2012, Acta Polytechnica, 52, 010000
Hartman, R. C., Bertsch, D. L., Bloom, S. D., et al. 1999, ApJS, 123, 79
Hartman, R. C., Kadler, M., & Tueller, J. 2008, ApJ, 688, 852
Jorstad, S. G., Marscher, A. P., Lister, M. L., et al. 2005, AJ, 130, 1418
Kataoka, J., Stawarz, L., Takahashi, Y., et al. 2011, ApJ, 740, 29
Koyama, K., Tsunemi, H., Dotani, T., et al. 2007, PASJ, 59, 23
Krawczynski, H., Hughes, S. B., Horan, D., et al. 2004, ApJ, 601, 151
Lebrun, F., Leray, J. P., Lavocat, P., et al. 2003, A&A, 411, L141
Lewis, K. T., Eracleous, M., Gliozzi, M., Sambruna, R. M., & Mushotzky, R. F. 2005, ApJ, 622, 816
Lichti, G. G., Bottacini, E., Ajello, M., et al. 2008, A&A, 486, 721
Linfield, R. & Perley, R. 1984, ApJ, 279, 60
Lubiński, P., Zdziarski, A. A., Walter, R., et al. 2010, MNRAS, 408, 1851
Magdziarz, P. & Zdziarski, A. A. 1995, MNRAS, 273, 837
Maraschi, L., Ghisellini, G., & Celotti, A. 1992, ApJ, 397, L5
Marscher, A. P., Jorstad, S. G., Gómez, J.-L., et al. 2002, Nature, 417, 625
Molina, M., Bassani, L., Malizia, A., et al. 2009, MNRAS, 399, 1293
Nolan, P. L., Abdo, A. A., Ackermann, M., et al. 2012, ApJS, 199, 31
Poutanen, J. & Svensson, R. 1996, ApJ, 470, 249
Predehl, P. & Schmitt, J. H. M. M. 1995, A&A, 293, 889
Rivers, E., Markowitz, A., & Rothschild, R. 2011, ApJS, 193, 3
Sargent, W. L. W. 1977, ApJ, 212, L105
Schlegel, D. J., Finkbeiner, D. P., & Davis, M. 1998, ApJ, 500, 525
Sguera, V., Bassani, L., Malizia, A., et al. 2005, A&A, 430, 107
Takahashi, T., Abe, K., Endo, M., et al. 2007, PASJ, 59, 35
Tavecchio, F., Maraschi, L., & Ghisellini, G. 1998, ApJ, 509, 608
Tombesi, F., Sambruna, R. M., Reeves, J. N., et al. 2010, ApJ, 719, 700
Tombesi, F., Sambruna, R. M., Reeves, J. N., Reynolds, C. S., & Braito, V. 2011, MNRAS, 418, L89
Tueller, J., Baumgartner, W. H., Markwardt, C. B., et al. 2010, ApJS, 186, 378
Urry, C. M. & Padovani, P. 1995, PASP, 107, 803